Intra-cardiac Impedance Reography Correlated with Pulse Oximetry and EASI-ECG Lead System

- Wireless Sensor Network for Biomedical Applications -

Bruno Miguel Gil Rosa

Instituto Superior Técnico, Av. Rovisco Pais 1, 1049-001 Lisboa, Portugal

Abstact – ***The goal of this work is to develop an integrated wireless network consisting of biomedical sensors for acquisition of physiological variables such as: electric potentials generated by the heart and recorded at the thorax surface, pulse oximetry of the finger and the measurement of biological tissues' impedance by reography.***

The present work was developed at Instituto de Telecomunicações as part of IST in a partnership with Instituto de Fisiologia from FML and it can have practical applications in healthcare monitoring units, eliminating the need for using physical connections between the patient and the recording equipment.

Keywords – ***Electrocardiogram, Pulse Oximetry, Biological Conductivity, Embedded Systems, Wireless Transmission, Digital Signal Conditioning.***

I - Introduction

The development of an integrated wireless network constitutes a step forward in what concerns the classical process of recording the human physiological variables. It is a very challenging and motivating task to build a system like this one which also has the ability to expand itself and incorporate new sensor nodes at anytime, thus, increasing the quantity of physiological variables recorded inside the network. The available data can then be intersected and physiological aspects revealed this way can be correlated.

Typical biomedical measurement systems include several electronic stages. The physiological process of interest is converted into an electric signal by the input transducer. Some analog signal processing is usually performed, often including amplification and filtering. Analog-to-digital conversion, signal storage and digital processing constitute to some extent the digital block for every biomedical sensor.

The transducer is often the most critical element in the system since it constitutes the interface between the patient and the rest of the electronic device [1]. The type of biotransducer used dictates most of the first analog stages of the block diagram. The energy that is converted by the input transducer may be generated by the physiological process itself as the case of electric potentials from the heart, indirectly related to the physiological process as pulse oximetry or produced by an external source as the case of impedance reography. So, the first stages in developing biomedical sensors are quite different and attention must be paid to the physiological variables involved in each measurement device.

The history of electrocardiography starts at the middle of the 19th century when British physiologists John Burden Sanderson and Fredrick Page recorded the heart's electrical current with a capillary electrometer that revealed the existence of two phases in the recordings, later called QRS and T. By the end of the century, Willem Einthoven started to improve the classical capillary electrometer building the first electrocardiograph machine by means of a spring galvanometer. He also introduced the term *electrocardiogram* (abbreviated to EKG or ECG) at a meeting of the Dutch Medical Association [2].

In 1912, Einthoven described an equilateral triangle formed by his standard leads I, II and III latter called "Einthoven's Triangle" which has guided him to win the Nobel Prize for inventing the ECG twelve years later.

In 1928 Ernestine and Levine reported the use of vacuum tubes to amplify the electrocardiogram instead of the mechanical amplification performed by string galvanometers. A further significant step was made after the invention of the cathode ray tube which allowed the manufacturing of cathode ray oscilloscopes. It improved considerably the physical characteristics of ECG recording and

new domains for electrocardiographic research such as vectorcardiography were opened.

The introduction of computers into electrocardiography soon replaced all the conventional ECG recording systems. At this point, recording time dependent signals without distortion is not anymore a major problem.

The first attempts to build pulse oximeters occurred in the 1930s and 40s by Carl Mathes and Glen Millikan [3]. The former built the first device to continuously measure blood oxygen saturation *in vivo* by transilluminating tissue while the latter used the term "oximeter" to describe a lightweight earpiece to detect the oxygen saturation of hemoglobin for use in aviation research.

In 1964, a surgeon Robert Shaw built a self-calibrating ear oximeter which was marketed by *Hewlett Packard*® in 1970 for use in physiology and cardiac catheterization laboratories.

In 1972, Aoyagi discovered that signals measured at two different wavelengths of light could be accurately related to oxygen levels in arterial blood [4]. Contemporary pulse oximeters rely on Aoyagi's theory and use two light-emitting diodes (abbreviated to LED) to generate large amounts of narrowband light that improve the signal quality.

The first publications concerning impedance plethysmography or reography date back to the 1930s and 1940s. In 1932 Atzler and Lehmann observed changes in the capacitance between two parallel plates kept across the human chest. These changes were observed to be synchronous with the activity of the heart. The technique as it exists today was first introduced by Jan Nyboer and co-workers in 1940 [5].

The method reached clinical value about 20 years ago based on the research work by Kinnen, Kubicek *et al* [6]. All these methods are based upon the placement of electrodes at the surface of the body while performing bioimpedance measurements inside body tissues as blood vessels and the heart constitutes a more subtle technique.

In 1980, Luís O. D. Amado published his doctoral dissertation under the topic of "Reografia Intracardíaca", translated to Intra-cardiac Reography, where he described that the volume of the four cardiac chambers could be rigorously measured with the reography method and using intracavitary catheters [7]. He also identified the major problems associated with this technique, in particular the weak capacity of the method in determining the absolute volume due to external factors like the geometry of the cardiac walls.

II – Material and Methods

The developed work consists of three different electronic devices. They are presented in different topics, starting by ECG recordings, followed by pulse oximetry and, finally, impedance reography measurements.

A – ECG Recordings.

The EASI lead system uses only four electrodes placed at anatomic points on the torso plus a ground electrode. This system has been evaluated to be less sensitive to noise and artifacts than the conventional twelve ECG leads [8]. The three bipolar leads of the EASI system are generated by pairwise subtraction of the potentials recorded at the E, A, S and I electrodes (*vid. fig. 1*), yielding three ECG leads:

. *Lead AI*, which records the electrical activity of the heart in a left-to-right direction;

. *Lead ES*, which records the electrical activity of the heart in a caudal-cranial direction;

. *Lead AS*, which records the electrical activity of the heart in an anterior-posterior direction;

Using the voltages from the bipolar leads of the EASI lead system as reference voltages, the voltage V_i of any arbitrary lead i is a linear combination of the voltages in leads ES, AS and AI, as shown in equation (1).

$$V_i = \alpha_i V_{ES} + \beta_i V_{AS} + \gamma_i V_{AI} \qquad (1)$$

This linear equation can be represented in terms of the constant dimensionless coefficients triplet (α_i, β_i, γ_i) [8]. The unknown values of the three coefficients can be determined by fitting them to the measured sets of voltages V_i, V_{ES}, V_{AS} and V_{AI}. This statistical approach is based under the assumption of the **dipole hypothesis** – the electrical activity of the heart can be represented by a single dipole or heart vector – and the linearity of the body's volume conductor.

The diagram block of the sensor device developed for ECG is shown in *fig. 2*. The remote sensor consists of an amplification stage performed by an instrumentation amplifier with high gain (500 V/V) after biopotentials been captured by conventional electrodes. These signals are converter to their digital form by a 3-channel 16-bit ADC with a sample rate of

1000 SPS *per* channel and configured in a ± 10 V bipolar input mode which gives an LSB of 302,2 µV. Some analog filtering is implemented between electrodes and the amplification stage: it includes a RFI filter at the input terminals of each instrumentation amplifier to limit the frequency range of common-mode input signals (<16 kHz) and an anti-aliasing filter with cut-off frequency around 500 Hz. This frequency is well above the frequency range of an ECG signal and the discrepancy seen between the bandwidth allowed and the sample rate of the ADC will provide greater detail level since there will be more data samples available to reconstruct the acquired ECG signal by interpolation or moving average techniques.

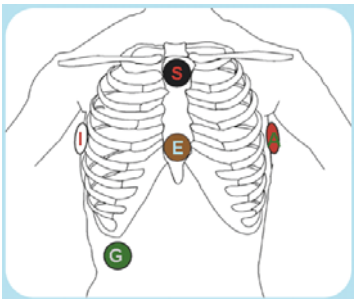

Figure 1 - Position of the electrodes in an EASI – ECG lead system. Translated from [9] with modifications.

The central processing unit of the ECG device is a 16-bit PIC microcontroller (abbreviated to PIC MCU) from *Microchip*® which controls all the operation for acquisition and storage of data samples with the help of an external timer. The digital interface with a radio frequency transceiver (abbreviated to RF transceiver) dictates the transmission of data from the sensor node to a remote recording one. The RF transceiver used transmits in the ISM frequency band of 2.4 GHz defined by the ZigBee™ Protocol.

Seeing that biopotential recordings necessitate a low impedance connection to be made to the patient, his safety has to be assured. The device is expected to transmit the measured potentials via wireless to the recording equipment so, it is not necessary a physical power line to feed the device and only a low voltage battery is used. This ensures the safety of the patient since he is no longer at risk of electric shock in the event of a fault from an equipment fed by power lines [1].

The reception of the data packets has revealed some limitations due to the fact that the real bandwidth involved in data exchange between remote nodes was only 4 kbps *per* channel. A bandwidth of 4 kbps means that only 250 data words can be received in every second. So, the maximum frequency component of the input signal recorded in these conditions is 125 Hz, 25 Hz below the maximum spectral component of an ECG signal. It might be sufficient to obtain an ECG recording with its features perfectly discernible, but, for higher rate sensors like reography, other communication solution must be found.

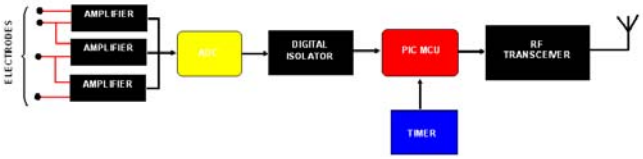

Figure 2 – Block diagram of the EASI - ECG device.

B – Oximetry Recordings.

Oxygen saturation which is often referred to as SaO_2 or SpO_2 is defined as the ratio of oxyhemoglobin (HbO_2) to the total concentration of hemoglobin present in the blood, i.e., oxyhemoglobin plus reduced hemoglobin:

$$SaO_2 = \frac{[HbO_2]}{[HbO_2]+[Hb]} \qquad (2)$$

Arterial SaO_2 is a parameter measured with oximetry and it is normally expressed as a percentage. Under normal physiological conditions arterial blood is 95% saturated, whilst venous blood is 75% saturated.

It is possible to use the differences in absorption spectra of HbO_2 and Hb for the measurement of arterial oxygen saturation *in vivo* because the wavelength range between 600 nm and 1000 nm is also the range for which there is least attenuation of light by body tissues. Tissue and pigmentation absorb blue, green and yellow light whereas water absorbs the longer infrared (abbreviated to IR) wavelength.

The two optimum wavelengths for pulse oximetry are in the red (λ_1 = 660 nm) and near infrared (λ_2 = 940 nm) regions. At 660 nm, reduced hemoglobin absorbs about ten times as much light as oxyhemoglobin while, at 940 nm, the absorption coefficient of oxyhemoglobin is greater than that of reduced hemoglobin. The pulse oximeter directly senses the absorption of red and infrared light and the ratio of pulsatile to non-pulsatile light at the red and infrared are translated through complex signal processing

techniques to a function of the arterial oxygen saturation [10].

Light propagation in a uniform medium is described by the *Beer-Lambert* law. According to it, the intensity I of the light in the medium is proportional to the transmitted intensity I_0 and decreases exponentially with the extinction coefficient of the absorbing medium ε, the concentration of the absorbing medium β and the path length L, according to equation (3).

$$I = I_0 \exp[-\varepsilon(\lambda)\beta L] \tag{3}$$

The unscattered absorbance, $A(\lambda)$, is given by taking the log of the transmitted intensity over the receiving intensity,

$$A(\lambda) = Ln(\frac{I}{I_0}) = -\varepsilon(\lambda)\beta L \tag{4}$$

and, for all the substances present in the medium, last expression becomes equation (5).

$$A_{total}(\lambda) = \sum_i \varepsilon(\lambda i)\beta i L \tag{5}$$

Both Hb and HbO_2 have different extinction coefficients at each wavelength. However, light is scattered in many directions as it enters the skin. Thus, light received by the photodetectors rarely travels in a straight path and it is heavily attenuated. The total absorbance at the two wavelengths in study is shown in equation (6) and (7).

$$A_{total}(\lambda 1) = (\varepsilon HbO2(\lambda 1)[HbO_2] + \varepsilon Hb(\lambda 1)[Hb])L \tag{6}$$

$$A_{total}(\lambda 2) = (\varepsilon HbO2(\lambda 2)[HbO_2] + \varepsilon Hb(\lambda 2)[Hb])L \tag{7}$$

In order to determine SaO_2, it is necessary to isolate the arterial component. By taking the time derivative of the absorption in equations (6) and (7) and assuming that only the blood path length – distance between the arterial vessel and the photodetector – changes, the ratio of the time derivatives gives equation (8).

$$R = \frac{\varepsilon HbO2(\lambda 1)[HbO_2]dL_{HbO2}/dt + \varepsilon Hb(\lambda 1)[Hb]dL_{Hb}/dt}{\varepsilon HbO2(\lambda 2)[HbO_2]dL_{HbO2}/dt + \varepsilon Hb(\lambda 2)[Hb]dL_{Hb}/dt} \tag{8}$$

Now, making a new assumption that vasodilatation (and vasoconstriction) of the arterial vessels are the same over the time, that is, $dLHbO_2 / dt = dLHb / dt$, last expression becomes equation (9).

$$R = \frac{\varepsilon HbO2(\lambda 1)[HbO_2] + \varepsilon Hb(\lambda 1)[Hb]}{\varepsilon HbO2(\lambda 2)[HbO_2] + \varepsilon Hb(\lambda 2)[Hb]} \tag{9}$$

The relationship between R and SaO_2 can then be written as equation (10).

$$SaO_2 = \frac{\varepsilon HbO2(\lambda 1) - R\varepsilon Hb(\lambda 2)}{(\varepsilon Hb(\lambda 1) - \varepsilon HbO2(\lambda 1)) - R(\varepsilon Hb(\lambda 2) - \varepsilon HbO2(\lambda 2))} \tag{10}$$

This last equation deviates slightly from theory. This happens because scattering effects have been ruled out from calculations; the spectrums of light sources that produce the two wavelengths are not a narrowed band and the assumption about the changes in path length is not absolutely true.

An empirical relationship between R and SaO_2 must, therefore, be determined for each particular sensor by plotting the R value against known-values of SaO_2. Within this approach, the R value is calculated by taking the normalized ratio of the red absorbances to the infrared ones. This normalized value is obtained by dividing the AC component of the absorbance at that frequency by the DC component as shown in equation (11), which is the same to take the time derivative of absorbances:

$$R = \frac{AC_{red} / DC_{red}}{AC_{ir} / DC_{ir}} \tag{11}$$

The remote sensor node developed for pulse oximetry is shown in *fig. 3*. It consists of an excitation circuit that produces voltage pulses for two light emitting diodes: one with a response in the red (660 nm) and the other one in the infrared (940 nm) spectrum. The LEDs are taken on alternatively for the corresponding photo-detector respond solely to it. The light beams that cross the finger and reach the detectors are converted to their digital form by a 2-channel 16-bit ADC. The sample rate is 12,5 kSPS *per* channel which allows to acquire alternatively and for a time period of 1 ms, five data samples when a pulse is taken on and twenty data samples when the pulse is off for background noise reduction.

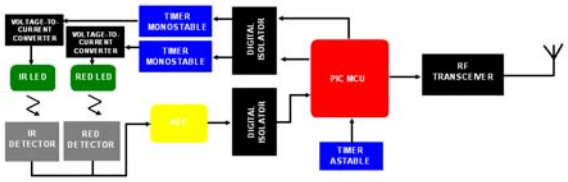

Figure 3 – Block diagram for the developed pulse oximeter.

Signal processing algorithms in pulse oximetry waveforms are typically applied in the time domain utilizing clustering and moving average (filtering) techniques.

The first algorithm used in this project to optimize this ratio was the clustering method, implemented inside the program memory of the PIC MCU.

A typical signal that comes from the photodetectors is shown in the top of *fig. 4*. As it can be seen, for the case of the infrared detection, the signal is corrupted with bands of data points that deviate up and down from the pulse oximetry curve. This noise can be eliminated using a clustering algorithm applied to the data that results from the analog-to-digital conversion and is temporarily available inside the data memory of the microcontroller.

The clustering algorithm developed for pulse oximetry consists of taking every five consecutive data samples from the ADC and to determine the respective median value. The reason to take the median value instead of the mean value is that the latter is more sensitive in the presence of extreme data values than the former one. So, by applying this algorithm is the same as doing a decimation process in the data sequence because from five data samples taken when a pulse signal is on, we ended up with only one data value and, from twenty data samples taken when a pulse is off, we get four data values. The overall sampling frequency is reduced from 25 kSPS to 5 kSPS.

As the PIC MCU has a limited instruction set, it was developed the simplest clustering algorithm possible to run inside the program memory without causing the microcontroller to stop executing instructions due to the complexity of the clustering code. So, the strategy adopted was to store every five consecutive binary samples inside a vector as soon as they were available and to perform a *bubble* sort to the vector. Finally, in the end of the processing, the median value can be read from the index position number three of the vector.

With all the median data points available it was performed one last operation inside the microcontroller: the median data point that corresponds to the pulse taking on was subtracted by the mean value of the four median data points that correspond to the pulse taking off in each time interval of 1 ms. Again, the overall sampling frequency is reduced to 1000 SPS and the difference signal can be seen in the bottom of *fig. 4*. It is the result of this subtraction that is stored in the transmission packet and subjected, after being received in the remote recording system, to the second signal processing algorithm – the moving average method.

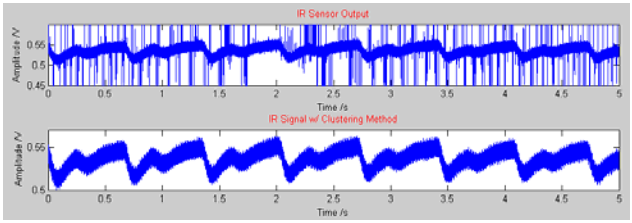

Figure 4 – Output signal that comes from the infrared detector (top). Infrared signal after the application of the clustering method (bottom).

The moving average algorithm is a time-discrete system defined mathematically as a transformation that maps an input sequence with values *x[n]* into an output sequence with values *y[n]* [11], and denoted according to equation (12).

$$y[n] = T\{x[n]\} \tag{12}$$

The value of the output sequence at each value of index *n* can depend on *x[n]* for some values of *n*. The general moving average system used in this project is defined by equation (13).

$$y[n] = \frac{1}{M_1 + M_2 + 1} \sum_{k=-M1}^{M2} x[n-k] \tag{13}$$

The system computes the *nth* sample of the output sequence as the average of $(M_1 + M_2 + 1)$ samples of the input sequence around the *nth* sample. The tested values for the algorithm that better fit to the typical pulse oximetry waveforms are $M_1 = 10$ and $M_2 = 10$.

The moving average algorithm just described is applied to the data received *via* wireless by the recording equipment because, as it can be seen, by applying this algorithm, the length of the output data sequence is not abruptly reduced as the case of clustering process. So it was worthless to order the PIC MCU to internally compute the moving average algorithm in a situation in which the transmission packet size wouldn't be reduced and it would certainly exist a remote processor in the recording equipment with a better

performance. In addition, the values for M_1 and M_2 can easily be changed in software, as the case of MATLAB®, running on the recording equipment. The result of the moving average algorithm is shown in top of *fig. 5*. It is this signal that is used for computation of the oxygen saturation level.

After signal processing and for visualization purposes only, the pulse waveform was subtracted by its mean value, followed by an inversion along the time axis for the signal resemble the typical pulse oximetry curve seen in clinical monitors.

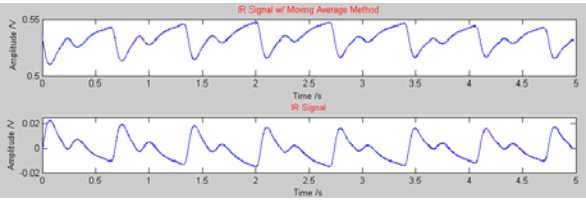

Figure 5 – Infrared signal after the application of the moving-average (top) and typical pulse oximetry curve (bottom).

Fast Fourier transformation (abbreviated to FFT) of time series oximetry waveforms has produced some important spectral components, as shown in *fig. 6* for the pulse signal with DC level and *fig. 7* for a more detailed signal around the DC level. These components are: a DC offset component at 0 Hz; a respiratory component at 0.2 Hz; an AC component at 1.5 Hz and its harmonics.

In computing the R value only the magnitudes of the DC and AC components detected in both red and infrared frequency spectrum are used, in accordance with equation (11). To do that, it was implemented in the recording equipment an algorithm that quickly calculates the mean value (DC) of both red and infrared signals and also searches for the maximum magnitude peak present within the cardiac physiologic spectrum of both signals, from 0.5 to 2.5 Hz, which corresponds to the pulsatile component of blood.

To obtain the real SaO_2 it was used the approximate formula: $SaO_2 = 110 - 25R$, from commercial pulse oximeters [13]. Of course, to reach a relative accurate value for the SaO_2 it would be necessary to run a calibration procedure with volunteers whose pulse saturation levels were known by a commercial pulse oximeter available and to adjust those values to the R ratio obtained with the developed device at the same time. A rigorous method to obtain an absolute accurate value for oxygen level saturation would consist in an intra-arterial catheter oximetry performed to volunteers.

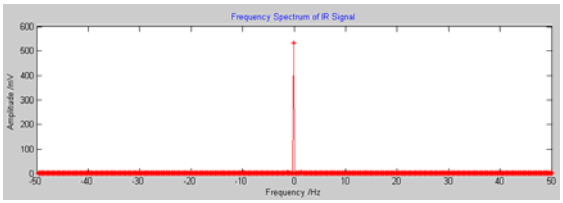

Figure 6 – Frequency spectrum of an oximetry waveform: DC offset is quite evident.

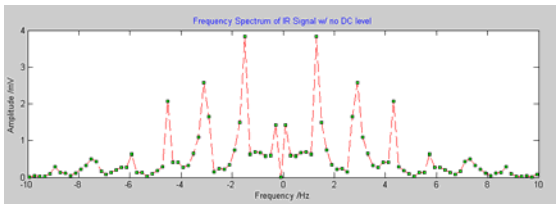

Figure 7 – A more detailed frequency content of the oximetry curve without the DC component.

C – Bioimpedance Recordings.

Biological tissues offer two types of resistance to an electric current: capacitive and resistive. The capacitive component arises from cell membranes and it is particularly important when electrodes are placed at the body surface. Skin is the main responsible for this capacitive resistance due to the keratinized layer that blocks DC and low frequency AC current. The conduction of high frequency AC current is made by capacitive effect that occurs between surface electrodes and the inner layers of the skin which have high conductivity.

The resistive component arises from extra and intracellular fluid. Bioimpedance value decreases when frequency goes higher which is reflected by a decrease of the value of reactance from cell membranes. At frequencies in the range of 20 kHz, membranes act as conductors of reactance even though skin still offers a considerable reactive component – this can be totally eliminated with frequencies above 100 kHz. Because of the weak capacitance of the biological tissues when working at 20 kHz, it is admissible to consider that, at that frequency, the current distributes itself through the tissue as it was a pure resistive element [5].

The developed prototype for reography consists of two separate circuits: one responsible for injecting the 20 kHz current sine-wave (as shown in *fig. 8*) while the other one senses and acquires data samples using a fast 18-bit ADC, *vid. fig. 9*.

The device solely permits to calculate the impedance module given that it only uses one acquisition channel that measures the voltages produced across the impedance segment.

Besides, all the available information from the injected current comes from theory, that is, it has 1 μA of amplitude and a frequency of 20 kHz. So, there is no way of estimating the value for impedance phase. This does not constitute a big issue because in calculating blood volume changes with respect to impedance ones, it is only necessary to know the module of the latter.

In order to compute impedance module, it was used equation (13).

$$|Z| = \frac{V_{r.m.s.}}{I_{r.m.s.}} \qquad (13)$$

The *r.m.s* value of a sine-wave signal is frequency and phase-independent and it is given by the ratio of the signal amplitude by the square root of 2. So, in what concerns the determination of the current signal's *r.m.s* value it was quite simple. For voltage it was used the mathematical formula for *r.m.s.*,

$$V_{r.m.s.} = \frac{\sqrt{\sum_i V_i^2}}{\sqrt{N}} \qquad (14)$$

where V_i constitutes the individual N voltage samples taken by the ADC, twenty samples in total for a period of 100 μS. Due to the fact that the PIC MCU only has 900 μs of available time to make all calculations and the fact that binary operations of square power and square root are very time and memory consuming processes, it was established that the microcontroller only has to compute equation (14).

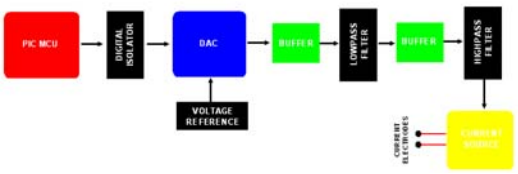

Figure 8 – Block diagram of the 20 kHz sine-wave generator circuit.

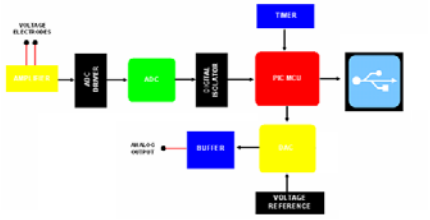

Figure 9 – Block diagram of the acquisition circuit used in reography.

The resulting voltage is then send via USB to a personal computer and the impedance module is finally calculated and corrected from parasite impedances developed throughout the sensing device.

The final stage for reography consists in calibrating the acquisition circuit with external resistors whose impedance values are known. As external resistors have a constant value of impedance, it is expected that the acquisition device will output a corresponding constant value for the r.m.s. voltage. Seeing that the r.m.s. value of a sinusoidal wave does not change within a period of the signal, the very fact of the injected current pass through a resistor will result in a sinusoidal voltage signal with constant r.m.s. voltage whose value is proportional to the resistor's impedance.

In order to obtain the proportional relationship between r.m.s. voltage and impedance, it was settled an experimental procedure consisting in recording the different voltage levels outputted by the acquisition system and match them to the values of resistors been tested. Figure 10 shows a recording performed this way. It can be seen four different steps corresponding to four different resistors as well as high step variations that occur anytime a resistor is taken from the feedback loop of the voltage-to-current source and current path is therefore open. The fit obtained will be used to test the reography device with NaCl solutions. The parameters of the fit are shown in *fig. 11*.

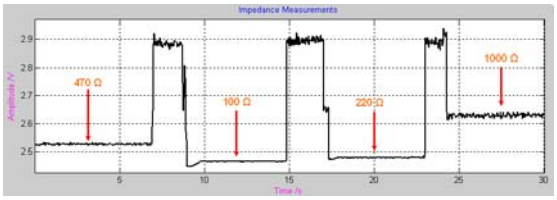

Figure 10 – Some impedance measurements performed with external resistors to calibrate the acquisition device.

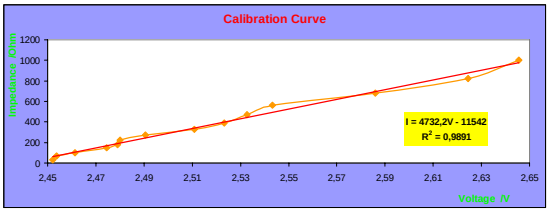

Figure 11 – Graphic showing the obtained fit between the computed r.m.s voltage given by the PIC MCU and the impedance values tested.

III – Results

A – ECG Recordings.

For ECG recordings, temporal samples were taken from every EASI system leads. Each lead records the potential differences between two points so, the deflections in each lead at any instant indicate the magnitude and direction of the cardiac vector. Figures 12 to 14 show temporal ECG recordings obtained with the developed device.

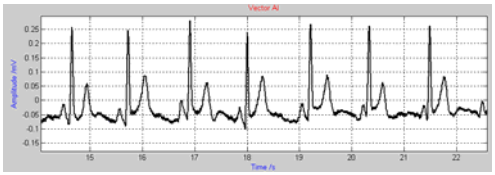

Figure 12 – ECG recording corresponding to the AI lead.

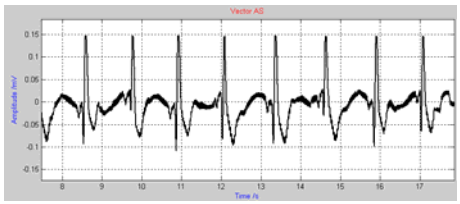

Figure 13 – ECG recording corresponding to the AS lead.

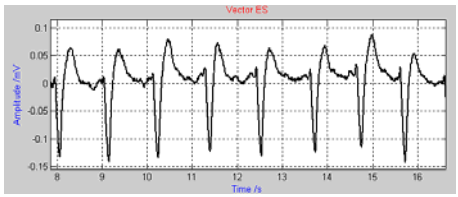

Figure 14 – ECG recording corresponding to the ES lead.

The device amplifies the difference between the electrode placed at the positive input terminal of the instrumentation amplifier and the electrode placed at the negative one.

The voltage convention adopted in the system was that of the electric circuits, that is, $V_{AI} = V_A - V_I$, $V_{AS} = V_A - V_S$, and $V_{ES} = V_E - V_S$. So, when a depolarization wavefront moves toward a positive electrode, it creates an upward deflection on the ECG in the corresponding lead whereas a downward deflection is created when a depolarization wavefront moves away from the positive electrode.

From the ECG curves, it can also be seen that there are seven QRS complexes reported in a time interval of 6 s which, extrapolating, gives a heart beat of 70 bpm.

B – Oximetry Recordings.

The first recording taken when the volunteer is breathing normally is shown in *fig. 15* as well as the corresponding SaO_2 rate during the experience in *fig. 16*.

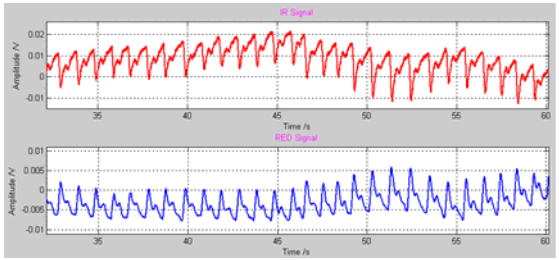

Figure 15 – Pulse oximetry curves obtained during normal breathing.

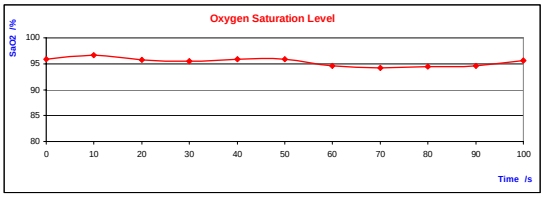

Figure 16 – Graphic showing the variation of the oxygen saturation level during normal breathing.

In these conditions, the blood is highly saturated ($SaO_2 > 95\%$) and oximetry curves are perfectly shaped.

During a forced breath-holding, the situation gets a little different as documented in *figs. 17* and *18*.

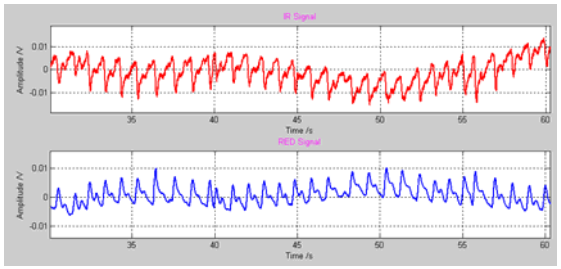

Figure 17 – Pulse oximetry curves obtained during forced breath-holding.

The oxygen saturation level dropped below 90% while pulse oximetry curves show an evident distortion in their normal contours. The reduction in the concentration levels of oxyhemoglobin results in a much higher

absorbance of red light by the reduced hemoglobin, causing the blood to get darker. An increase in red light absorbance means that less amounts of red light will reach the corresponding photodetector. A critical drop in the DC component of the red signal will increase the *R* value which, by its turn, lowers the SaO_2 percentage.

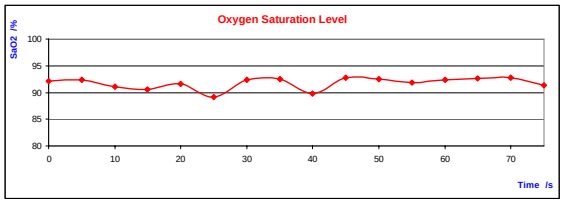

Figure 18 – Graphic showing the variation of the oxygen saturation level during normal forced breath-holding.

C – Bioimpedance Recordings.

In this section, it is presented the results obtained with the reography prototype for NaCl solutions whose conductivity differs between them. Figures 19 to 20 show temporal impedance recordings performed by the developed reography device.

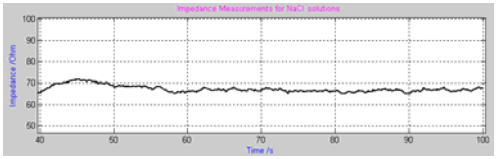

Figure 19 – Impedance measurements obtained for a NaCl solution with 12880 µS cm^{-1} of conductivity.

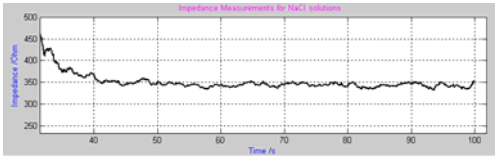

Figure 20 – Impedance measurements obtained for a NaCl solution with 2764 µS cm^{-1} of conductivity.

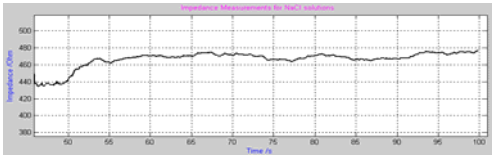

Figure 21 – Impedance measurements obtained for a NaCl solution with 2070 µS cm^{-1} of conductivity.

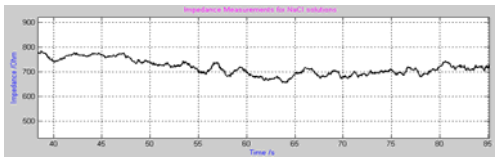

Figure 22 – Impedance measurements obtained for a NaCl solution with 1413 µS cm^{-1} of conductivity.

Since the path length between the sensing electrodes is 1 cm and the units for conductivity are presented in µS cm^{-1}, the corresponding impedance value is straightforwardly identified by the inverse of the solution's conductivity.

The curves shown are close enough to the impedance values that were expected to obtain by theory. These values are: 708 Ω for the NaCl solution whose conductivity is 1413 µS cm^{-1}, 483 Ω for the solution with conductivity 2070 µS cm^{-1}, 362 Ω for 2764 µS cm^{-1} and 78 Ω for conductivity 12880 µS cm^{-1}.

The impedance curves obtained show some variation around the central line but, more importantly, they are quite discernible and blood conductivity is in the middle range of them (6800 µS cm^{-1}).

IV – Conclusion

A – Considerations about the developed work.

The electronic prototype on pulse oximetry recordings is completely finished as well as all the algorithms involved in their acquisition and processing stages at the remote node and in the central recording system. For ECG, the substitution of the RF transceivers by other ones with higher bandwidth even inside the ZigBee Protocol is crucial to cover the entire frequency spectrum of the signal, in particular the fast transitions seen in the QRS complex.

By its turn and besides obtaining already some satisfactory results, the prototype developed for reography still needs more experimental tests to assess its performance at full operation in medical environment. The prototype has already proved that it can measure the impedance values of external resistors as well as NaCl solutions with different conductivities. However, due to the lack of information about intra-cardiac reographic curves that are expected to obtain during a cardiac cycle, it is difficult to establish an upper limit (if there is any) to the impedance value

that can be recorded by a reographic device: in fact, the prototype is not able to accommodate all the voltage levels that can be developed across the impedance segment and if some of them exceeds the projected ranges, the amplifiers will certainly saturate, damaging the recordings. Another technical aspect to be taken in count is to replace the USB communication by RF transceivers with higher bandwidth for data exchange than those used in this project. Because of time constrictions, this solution was not possible to be answered and it will remain a topic for future work.

B - Guidelines for Future Projects.

Every electronic project is subjected to continuous updating. The network protocol can remain the same while new remote notes can be progressively built and then fully integrated in the wireless system. The network can be increased in what concerns the number of member nodes and radio range if router nodes are available. Hospital healthcare units equipped with a system like this can record all the physiological variables of interest from the patient and send them with no physical connection to a central recording system or a personal digital assistant (PDA) of a clinician. One area of particular interest is that one that is concerned in building home-monitoring equipments so the patient can rest and recover at home while his physiological parameters are been sensed. Then, a remote recording system would send them through the internet to hospitals or particular clinics.

ECG recordings can be improved using a new acquisition paradigm based on the utilization of capacitive electrodes instead of the conventional ones. Within this approach, the body surface will act as a plate of a capacitor while the other one will be the terminal input of an instrumentation amplifier with high impedance. Therefore, on every potential point in the human body surface, a sensor of this type can be placed with extensive capability to perform *in situ* both analog-to-digital conversion and wireless transmission processes.

For pulse oximetry, one of the aspects that can constitute a target for innovation is to use more than two photoemitters to cover the maximum extension of the absorption spectrum of hemoglobin as possible. With more information about the light absorption and transmission at different wavelengths, the oxygen saturation level can be obtained more accurately. The replacement of the two LEDs by LASER – Light Amplification by Stimulated Emission of Radiation – technology would also constitute an innovation because instead of having light sources that irradiate light in all directions, the laser system would produce a direct beam of light, reducing the scattering effects that result from penetrating the finger. The pulse oximetry waveforms would show up with better shape in the recordings without the risk of occurring photoablation if the beam intensity is controlled.

Finally, the fundamental developments to perform over reography are the following ones: to build an intra-cardiac probe insensitive to external variations that measures the absolute volume of the cardiac cavities by performing impedance measurements; to establish an electromagnetic model of the walls of the cardiac cavities; and to eliminate the need for surgical catheterization by performing measurements using Magnetic Induction Tomography when the intra-cardiac impedance map is intended to be known.

V – References

[1] Jennings, D. *et al.*, *Introduction to Medical Electronics Applications*, Edward Arnold, London, 1995.

[2] Zywietz, C., *A Brief History of Electrocardiography – Progress through Technology*, Biosignal Institute for Biosignal Processing and Systems Research, Hannover.

[3] Kästle, S. *et al.*, *A New Family of Sensors for Pulse Oximetry*, Hewlett-Packard Journal, Article 7, February 1997.

[4] Bell, C., *Understanding Contemporary Pulse Oximetry*, GE Healthcare – Clinical Paper, 2005.

[5] Kyle, G. U. *et al.*, *Bioelectrical Impedance Analysis – part I: review of principles and methods*, Elsevier, No. 23, pp. 1226 – 1243, 2004.

[6] Jindal, G. D. *et al.*, *25 Years of Impedance Plethysmography*, Barc Newsletter, No. 236, September 2003.

[7] Amado, L. O. D., *Reografia Intracardíaca. Fundamentos teóricos e experimentais e algumas das suas contribuições hemodinâmicas*, Dissertação de Doutoramento apresentada à Faculdade de Medicina de Lisboa, Lisboa, 1980.

[8] Klein, M. D., Key-Brothers, I., Feldman, C. L., *Can the Vectorcardiographically Derived EASI ECG be a Suitable Surrogate for the Standard ECG in Selected Circumstances*, IEEE Computers in Cardiology, Vol. 24, 1997.

[9] Jahrsdoerfer, M., Giuliano, K., Stephens, D., *Clinical Usefulness of the EASI 12-lead Continuous Electrocardiographic Monitoring System*, Critical Care Nurses, No. 25, pp. 28 – 37, October 2005.

[10] Kamat, V., *Pulse Oximetry*, Indian Journal of Anaesthesia, No. 46, pp. 261 – 268, 2002.

[11] Semmlow, J. L., *Biosignal and Biomedical Image Processing. MATLAB – Based Applications*, Marcel Dekker Inc., New York, 2004.